Proceedings of the 34th IEEE/ACM Design Automation Converence, Anaheim CA, June 9-13, 1997, Best Paper Award

Computer-Aided Design of Free-Space Opto-Electronic Systems

S. P. Levitan[✣], P. J. Marchand[✦], T. P. Kurzweg[✣], M. A. Rempel[✣]
D. M. Chiarulli[✣], C. Fan[✦], F. B. McCormick[✦]

[✣]University of Pittsburgh
[✦]University of California, San Diego

Abstract

This paper presents a system capable of static and dynamic simulations of heterogeneous opto-electronic systems. It is capable of modeling Gaussian optical signal propagation with mechanical tolerancing at the system level. We present results which demonstrate the system's ability to predict the effects of various component parameters, such as detector geometry, and system level parameters, such as alignment tolerances, on system performance.

1. Introduction

Free space opto-electronic (FS-O/E) information processing systems are key components of the next generation of computers and communications networks. Currently the "state of the art" for design and analysis of these systems is to use a set of ad-hoc procedures to generate end-to-end system performance estimates based on empirical characterizations of the component devices. This painstaking technique results in rough approximations which must then be refined by actually prototyping each of the particular systems under consideration. As a result, while many systems have been proposed, few FS-O/E systems have been designed, and fewer still have been built. This is in sharp contrast to the growth of rapid prototyping systems in the electronic (VLSI) domain, where the path from concept to system is often as short as a few weeks.

The basis for this problem become clear when we look at an example of a prototypical opto-electronic system as shown in Figure 1. This figure shows a simple system consisting of a digital logic module interfaced to a vertical cavity surface emitting laser (VCSEL) array that supports parallel information channels. These are switched by a spatial light modulator (SLM) and directed to a detector array where the channels are received and passed on to another digital sub-system. The two digital sub-systems could be composed of simple logic modules, or could be as complex as an array of processing elements (*i.e.*, CPUs), making the system a tightly coupled parallel processor. In this case, the opto-electronics would provide high bandwidth channels between the processors [3] [13]. Over the past decade, many hybrid systems of this type have been proposed for applications as diverse as Multistage Interconnection Networks, Crossbar Switches, Intelligent Optical Backplanes, Optical Neural Systems, 3-D Digital Optical Computers, and Analog Optical Processors [1] [8].

The design of these complex systems has been impeded because currently, there are no O/E system level modeling tools. To date, there has been some work on CAD systems exclusively for fiber networks [4]. Other researchers have focused on mechanical issues [19]. Also, several researchers have proposed to implement systems level tools by extending an existing simulation language such as VHDL [6], SPICE [16], or by using a prototype microelectronics CAD tool such as Genesys [5]. Other groups have built their work on extending signal propagation models [12] or device models [11] [18]. The problems with these techniques come from the limitations imposed by trying to extend available tools beyond their original capabilities. It is difficult to successfully generalize these tools for a wide range of opto-electronic system level concerns.

In contrast, we have created a framework, as well as simulation and analysis tools, that use system level models of opto-electronic components. The framework provides bridges to specialized tools with analysis filters to sort and aggregate their results [10]. The simulation tool provides system level simulation and analysis for opto-electronic devices (e.g., modulators and sources) with a high level optical system simulator based on Gaussian beam propagation. It is this system level simulation tool which is the focus of this paper.

The remainder of this paper is organized as follows. We first present some background on the models necessary in O/E system level design. We then show the results of our modeling efforts for O/E signals and components, appropriate for system simulation. We continue by presenting results from static and dynamic simulations of a simple system and show how our tool can be used to perform technological and architectural trade-offs. We conclude with our plans for future work.

2. System Level Models

A system level model can be defined in terms of its models for "modules", the "signals" which pass between them, and the "dynamics" of the system behavior. For O/E systems our signals are electronic as well as modulated carriers, i.e., beams of light. The characteristics of this carrier are as important to model as the signal itself. Therefore, we need to have a flexible model for the propagation of optical signals. Using the characteristics of both the optical and electronic signals which carry information between the components, we can then define models for the system component modules in terms of the ways they transform the characteristic parameters of these signals. Finally, our model of the dynamic system behavior is based on a time domain analysis of the propagation of the signals through the components.

We first review some basic properties of optical signals and then present the Gaussian models we use to model propagation, power, tolerancing, and clipping of optical signals for free space O/E systems.

2.1 Propagation Models for Optical Signals

There is a range of abstractions which could be used for modeling optical signal propagation [17]. The most basic model is ray optics, or geometrical optics, where we use simple geometry and the normal of the propagating wave. More detail can be gained using Gaussian beams, which are models of paraxial waves, a simplification of more general wave optics, which use

DAC 97, Anaheim, California
(c) 1997 ACM 0-89791-920-3/97/06 ..$3.50

scalar waves to model propagation. An even more general model is electromagnetic optics where the true E/M fields are directly modeled. Finally, quantum optics, or quantum electrodynamics, are required to model propagation in certain non-linear optical materials. For system level design and analysis, ray optics are appropriate for the most basic models, while Gaussian beam optics models are more appropriate for typical FS-O/E system applications.

2.1.1 Geometric Propagation Models

For simple approximations, which do not consider phase, polarization, wavelength or intensity, we can use the most basic model of propagation, ray optics. We present a brief description of both optical signal propagation and ideal optical device models below.

For this discussion we assume that light is propagating in the positive z direction. An ideal ray of light at any point along the z axis is characterized by its x, y position and its ρ and θ angles with the z axis in the x and y planes. The geometric transformations performed on this ray by its passing through linear, ideal optical components can be captured in the simple 2-D ray transfer matrix **M**:

$$\textbf{(1)} \qquad \begin{bmatrix} y' \\ \theta' \end{bmatrix} = M \begin{bmatrix} y \\ \theta \end{bmatrix} \qquad \begin{bmatrix} x' \\ \rho' \end{bmatrix} = M \begin{bmatrix} x \\ \rho \end{bmatrix}$$

Analogous to the transformation matrices used in graphics and image processing, propagation through multiple or cascaded components can be modeled by a concatenation of multiplications. These geometric models give some insight into the physical (3-D) configuration of opto-electronic systems. However, they do not handle many important issues essential to designing the non-ideal and non-linear devices needed for information processing systems.

2.1.2 Gaussian Propagation Models

For modeling non-ideal sources that generate wavefronts making small angles to the z axis, such as laser sources, we use a Gaussian beam approximation. Here we minimally introduce parameters for the wavelength, λ, the beam waist (or spot radius), *W*, the Rayleigh range (or depth of focus), z_0, and the intensity of the light. Using the abstraction of a "beam," we can still model the propagation of the center of the beam using the algebra for geometric propagation of rays, with the addition of equations for the transformations for the intensity and beam waist for each component. Further, we must add a notion of optical power. Optical power is the integral of the intensity of the beam over the area of incidence. In the ideal case, beams are narrow and physically far apart. In practical systems, beams disperse, and arrays of beams travel through common components. The beams are detected by arrays of detectors where practical constraints on component sizes and spacing makes the overlapping of beams non-negligible, leading to cross talk.

However, the Gaussian beam approximation fails when the beams are clipped by the optical components through which they pass. In those cases, the equations for intensity and beam waist break down. Breakdowns can occur for systems with arrays of microlenses, or lenslets, where logical or physical constraints cause splitting or clipping of the Gaussian beams.

Clipping a Gaussian beam through a circular aperture gives a power loss related to the size of the aperture:

$$\textbf{(2)} \qquad P_{new} = P\left(1 - e^{-2k^2}\right)$$

where $k = D_{apt}/(2W_{apt})$ is the ratio of the diameter of the aperture to the beam waist size at the aperture. For $k > 2.12$ the clipping is less than 0.1% and can be ignored. For severe clipping ($k \le 1$) the Gaussian approximation breaks down completely. For moderate clipping ($1 < k \le 2.12$), the diffractive effects can be modeled as shown below. In this range, the power loss varies from 13% to 0.1%. However, the loss in power is not the most significant change. Clipping the beam also distorts its shape [14]. The change in shape can be modeled by using a new Gaussian beam with a new "effective" beam waist:

$$\textbf{(3)} \qquad W_{0eff} = W_0(1 - e^{-k^2}) \cdot \cos(pk^2/(2\pi))$$

where W_o is the initial waist, $p = 2\pi(z/z_0)$, z is the distance from that waist to the aperture, and z_0 is the initial Rayleigh range. The effective waist can vary by $\pm 36.8\% < W_{0eff} < \pm 1.12\%$ relative to the initial waist for $1 < k \le 2.12$. The new "effective" Rayleigh range is then:

$$\textbf{(4)} \qquad z_{0eff} = \frac{\pi W_{0eff}^{\ 2}}{\lambda}$$

which means that the beam divergence can vary from the original by as much as: $\pm 60.0\% < z_{0eff} < \pm 2.23\%$ for $1 < k \le 2.12$.

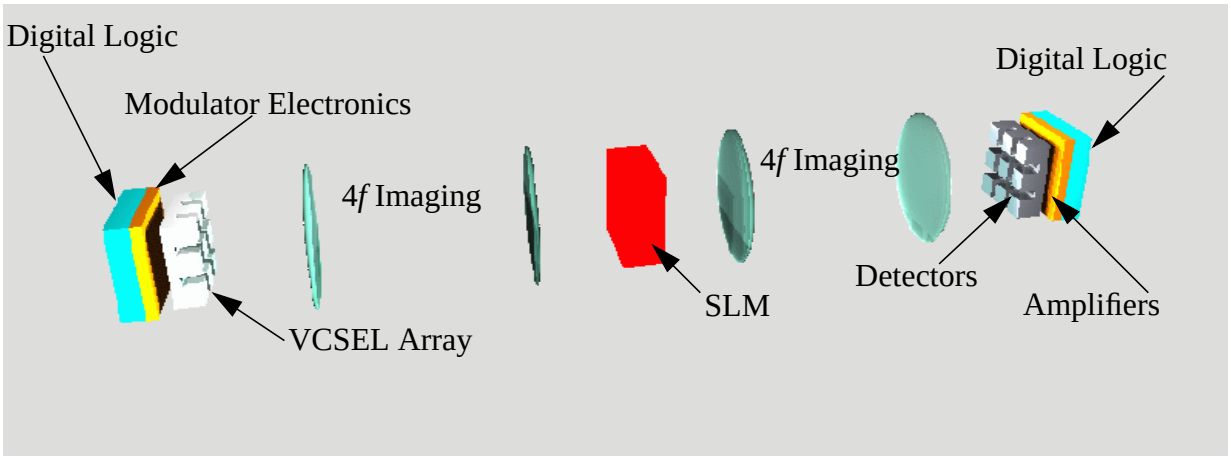

Figure 1: FS-O/E System

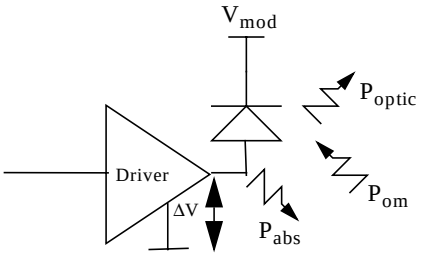

Figure 2: Generic Electro-Optic Modulator

While the total power will be decreased by the clipping at the aperture, it is interesting to note that the cosine term can be either positive or negative allowing the effective waist to become either larger or smaller than the initial waist. With the combination of the new power, effective waist, and effective Rayleigh range, a new Gaussian beam can be used in place of the original.

2.2 Device Models

Continuing our presentation of our electro-optic models, we move to active device models for transmitters and receivers. While these models are also approximations, they are accurate at the level of abstraction required for system level design and analysis.

2.2.1 Transmitters

Transmitters can be either based on an emitting source technology, such as VCSELs [9], or a modulation technology, such as multiple quantum well (MQW) modulators [15].

Figure 2 shows driver electronics and a MQW modulator reflecting a portion of the incident light, P_{om}, as modulated optical power, P_{optic}. Both reflective and transmissive modulators are possible. In either case, the key parameter is the amount of optical power which is absorbed by the modulator as a function of the controlling voltage. Equation 5 shows a model of the relationship of input modulation voltage to absorbed optical power for the MQW modulator. In this example, the modulator absorbs a fraction of the input optical power and reflects the rest. The relationship of the modulation voltage to absorbed optical power is modeled using a Lorentzian lineshape:

$$\textbf{(5)}\quad P_{abs}(V) = \frac{P_{om}k(V)}{1+\dfrac{P_{om}}{A\cdot I_s(V)}} \qquad \textbf{(6)}\quad P_{optic} = P_{om} - P_{abs}$$

The functions k(V) and I_s(V) for the knee and saturation current are interpolated from empirical measurements and A is the area of the modulator [7]. Figure 3 shows this relationship for typical values of incident optical power and modulation voltage.

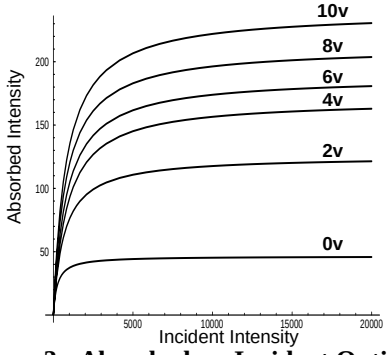

Figure 3: Absorbed vs. Incident Optical Intensity in W/cm^2

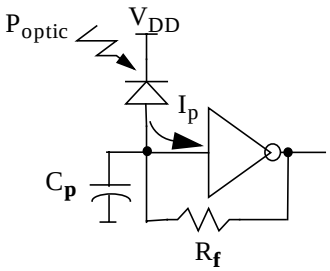

Figure 4: Single Stage Transimpedence Receiver

Equation 6 shows the relationship of incident power to reflected power. Note that the reflected optical intensity is the inverse of the electrical modulation signal.

Alternatively, VCSELs generate optical beams directly with a power dependent upon the input drive electrical power. We model our VCSELs as in Equation 7.

$$\textbf{(7)}\quad P_{out} = \frac{(\eta_{LI}/V_{th})}{(1-\eta_{LI}/V_{th})}\cdot(P_{in} - V_{th}I_{th})$$

where I_{th} is the laser threshold current, V_{th} is the laser threshold voltage, η_{th} is the laser L-I slope efficiency, and P_{in} is the input power.

2.2.2 Receivers

A generic single ended receiver is shown in Figure 4. The two primary components are a photo-diode and a transimpedence amplifier. This circuit was modeled and simulated with SPICE, and the characteristic parameters were extracted and used to define the transfer function for system level simulation. Equation 8 shows our model of the detector in the s-domain. We use the Laplacian transfer function for a transimpedence amplifier with a feedback resistance, where *R* is the total resistance, *C* is the total capacitance, and *A* is the gain of the amplifier.

$$\textbf{(8)}\quad \frac{H_{out}(s)}{H_{in}(s)} = \frac{R}{(1+(RC/A)s)}$$

Equation 9, uses this transfer equation to give the relationship of the input optical power to the output voltage for the photo-diode, single stage transimpedence amplifier receiver.

$$\textbf{(9)}\quad V_o(s) = \frac{R_f}{1+\left(\dfrac{R_fC}{A}\right)s}\cdot P_{optic}(s)$$

Taking the inverse Laplacian, the function can be represented in the time domain. The voltage output function is dependent on both the signal input and the state of the transimpedence amplifier. Using a piece-wise linear waveform, the final equation in the time domain is then:

$$\textbf{(10)}\quad V_{out}(t+\Delta t) = XR\left[\frac{RC}{A}(e^{-y}-1)+\Delta t\right] + P_{in}(t)R[1-e^{-y}] + V_{out}(t)e^{-y}$$

where $X = (P_{in}(t+\Delta t) - P_{in}(t))/(\Delta t)$ and $y = \Delta t(A/(RC))$

We use this same method to approximate the dynamic response of each of the modules in the system. For simulation, the number of points in the piece-wise approximation is a user defined variable.

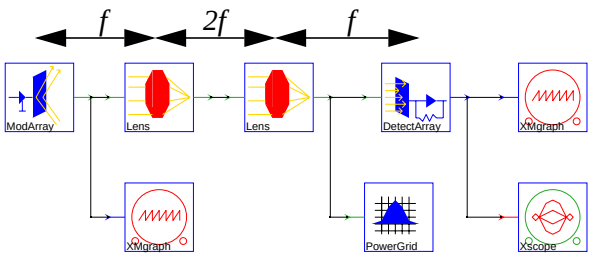

Figure 5: Ptolemy *4f* end-to-end simulation

3. Simulation Results

In addition to transmitters and receivers, we have built models for a number of other active and passive optical components. We have incorporated these models, into a prototype functional simulation system based on Ptolemy - a simulation system developed under the RASSP program by researchers at U.C. Berkeley [2]. Ptolemy is a generalized simulation framework used for rapid prototyping of digital signal processing systems. Using the synchronous data flow domain (SDF) in Ptolemy, we have defined our own message class, which is derived from the Ptolemy message class, to support both geometric and Gaussian propagation of light.

Figure 5 shows a simple system as modeled in Ptolemy. Each icon, or "star," represents a basic opto-electronic component or input/output function. The **ModArray** input star allows us to simulate arrays of arbitrary data patterns that are modulated onto an array of laser light beams. The **XMgraph** output star displays either the voltage or optical intensity of a single pixel during simulation. For the simulations, the **ModArray** interpolates a sequence of arrays of bit patterns (read from a file) into piecewise linear voltage waveforms that drive the modulator models described above. The resulting optical intensity waveform is passed through the lens models using the Gaussian propagation equations. The **PowerGrid** star is used to observe power in a cross-section of the optical signals. Additionally, it can show the placement and power received by a set of ideal detectors. On the other hand, the **DetectArray** star models the dynamics of the receiver models by first integrating the intensity from each Gaussian beam over the area of each detector, and then transforming the piece-wise linear optical power waveforms into voltages using the s-domain model as shown above.

In the next sections, we present three sets of simulation results. First, we show a static power analysis of beams propagating from transmitter to receiver. Next, we give an analysis of the Gaussian clipping behavior. Finally, we present a dynamic simulation of a single bit propagating through a point to point link.

3.1 Static Simulation

Figure 6 shows the results of combining the modulator and receiver models. Figure 6(A) graphically illustrates the modulation voltages for a 3×3, 20μm spotsize, 40μm spacing, MQW modulator array. Black squares represent 0 Volts and white squares represent 10V modulation. The source power comes from nine 1mW spots generated by a 850nm laser. The table under A shows the optical power reflected by each of the modulators. The table also shows the lack of modulation depth (a contrast ratio of 1.17 or about 1.4db) typical of MQW modulators. Figure 6(B-F) show images of Gaussian beams superimposed on an array of detectors after the light has passed through a *"4f"* imaging lens system. The tables below the figures show the corresponding power, in μWatts, at the detectors. The *"4f"* system consists of two lenses with focal length *f*. The first lens is placed *f* away from the input, the second lens is placed *2f* from the first, and the detector array is placed *f* beyond the second lens.

In all the figures, one can see the Gaussian intensity profile of the 20μm beams. Note that the image is inverted in intensity, due to the inverting properties of the modulators, and is inverted spatially, due to the lens system. Figure 6(B) shows the array of modulated beams imaging on an array of detectors where the photo-diode of each detector is 5μm × 5μm. Figure 6(C), (D), and (E) show 10μm × 10μm, 20μm × 20μm, and 35μm × 35μm detectors respectively. Note that for the 35μm detectors, almost all of the power from the modulators is recovered. Figure 6(F) shows the power detected by the 20μm × 20μm detector array for the case that the second lens of the 4*f* system has a small (10μm) mis-alignment in both x and y positions. This shows how the static simulations can be used to estimate the required mechanical tolerances of O/E systems.

3.2 Clipping Results

When examining lenslet systems, where the size of the lenses themselves are on the order of the dimensions of the Gaussian beams (5-40μm), we must concern ourselves with clipping as well as mis-alignment and tolerancing. In this case, each lenslet can act as an aperture and the clipping equations become relevant. Table 1 shows a comparison between output powers for a clipped and an unclipped array of spots. For this simulation we used a 10μm spot, 30μm spaced, source array for the MQW modulators at a wavelength of 850nm. The modulator array was

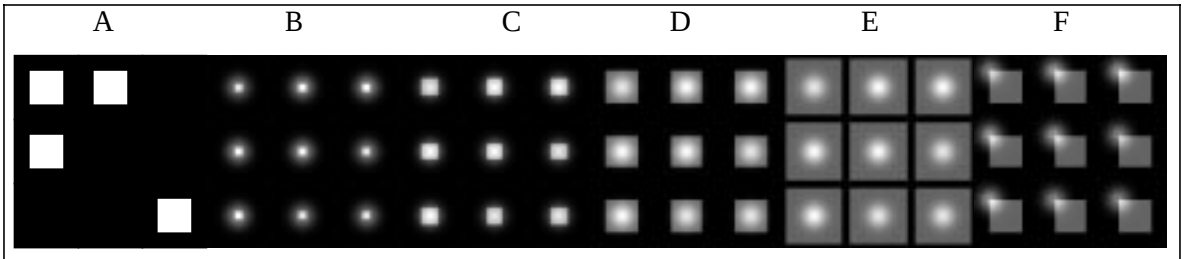

20μm Modulators			5μm Detectors			10μm Detectors			20μm Detectors			35μm Detectors			Misaligned Lens		
771	771	906	113	133	133	360	422	422	703	826	826	771	905	905	193	227	227
771	906	906	133	133	113	422	422	360	826	826	703	905	905	771	227	227	193
906	906	771	133	113	113	422	360	360	826	703	703	905	771	771	227	193	193

Figure 6: Power in μWatts Detected at Different Sized Detectors

100µm from the lenslet array, which had a focal length of 50µm. The detectors were placed 100µm behind the lenslet array. By varying the lenslet diameter from 33µm to 15µm we simulate the input beam being clipped by various amounts.

Table 1: Clipping results: 10µm Spot Sources, Varying Lenslet Diameters

Lenslet Diameter	33µm	22µm	15µm
k ratio (at Lens)	2.24	1.49	1.02
W_{0eff}	$5.00x10^{-6}$	$5.40x10^{-6}$	$4.23x10^{-6}$
z_{0eff}	$9.24x10^{-5}$	$1.08x10^{-4}$	$6.61x10^{-5}$
% Power Clipped	0%	1.2%	12.5%
Spotsize at Det.(µm)	10.02	10.80	8.46
% Loss w 20µm Det.	0%	1.21%	12.58%
% Loss w10µm Det.	8.83%	13.5%	15.72%
% Normalized Loss	0%	5.1%	7.5%

The table shows that for the 33µm lens, k is greater than 2.12 and no power is lost due to clipping. For the 22µm lens, the k ratio is 1.49 and the power clipped by the aperture is 1.2%. Using the 15µm lens, the k ratio is 1.02 and the power clipped by this aperture is 12.5%. However, more interesting are the effects at the detectors due to the changes in the beam shapes. In the process of clipping the beam, both the 15µm and 22µm lenslet arrays distort the shape of their beams. These distortions are shown in Table 1 as the effective waist and the effective Rayleigh range. The 15µm lens effectively decreases the spot size at the detector array, while the 22µm lens increases the spot size. This is due to the cosine function in Equation 3. For Gaussian beams, 86% of the power is carried in the waist (the radius of the spotsize), and 99% of the power is found in a circle with a radius of 1.5 times the waist. For the 15µm lens beam, most of the power of the beam in carried in a spot that can be detected by both the 20µm and 10µm detectors, whereas for the 22µm lens beam, the spotsize is larger than the 10µm detector, and a significant amount of additional power is lost. This is more evident when we normalize the detected power at the 10µm detectors to the power for the unclipped beam.

3.3 Dynamic Simulations

The system shown in Figure 5 can also be used to perform dynamic simulations. Figure 7 shows one piece-wise linear signal at the two **XMgraph** monitor points: the output of one of the modulators, showing intensity in W/m^2, and the output of one of the detectors, in Volts. Figure 7(A) shows operation at 100MHz, and Figure 7(B) shows bit rates of 300MHz. Here, the detectors were each 40µm and the receiver model parameters were A=1, R=4kΩ and C=250fF. The **Xscope** output star shows a voltage "eye" diagram for this random sequence of bits. Eye diagrams can be used for determining timing jitter as well as noise margins. For example, we can see in Figure 7(B) that from 100MHz to 300MHz the noise margin, defined as the ratio V1/V2, has dropped from 96% down to 52%. This is an example of how a functional model can give parametric results on system performance.

Figure 8 shows a second simulation, where we use eye-diagrams to illustrate the trade-offs between detector size, power detected, and noise margins. Figure 8(A) is the output from the same 5µm detector system shown in Figure 7(B). Figure 8(B) shows the output of one 20µm detector from the mis-aligned system in Figure 6(F). The smaller detectors are faster, with an effective C_p of 100fF, while the larger detectors capture more power (shown here as output voltage) but are slower due to an effective capacitance of 150fF. At 300MHz, this gives the faster detectors an 80% noise margin, compared to only 50% for the

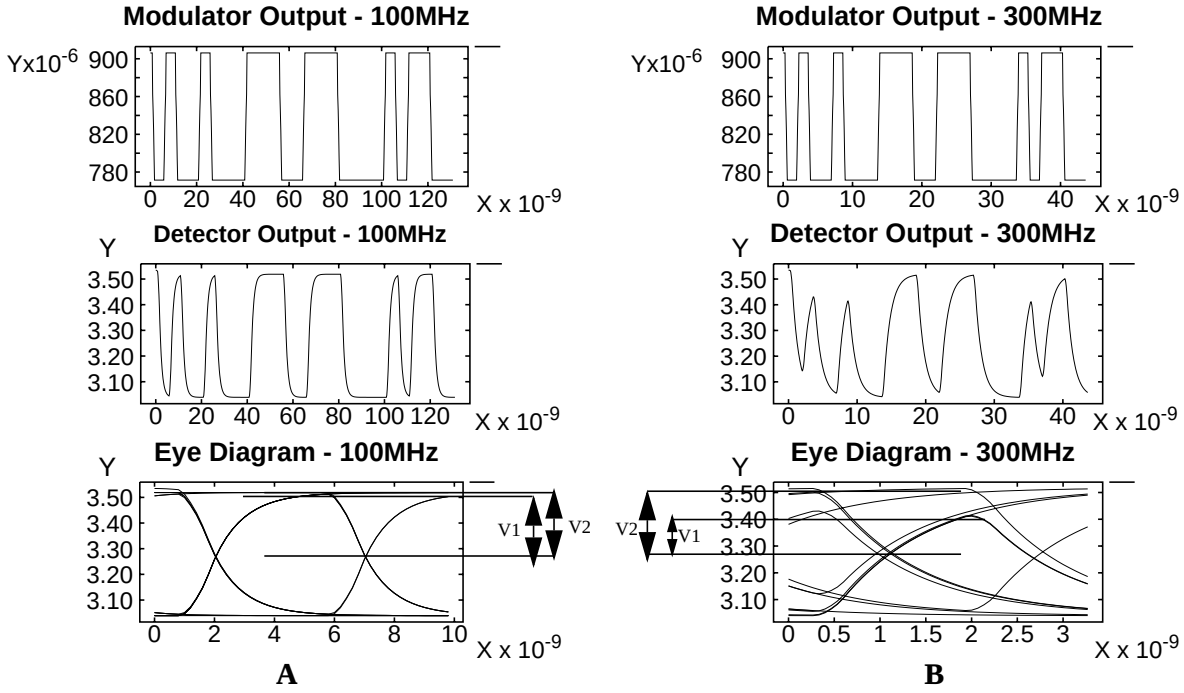

Figure 7: Modulator/Detector single channel simulations

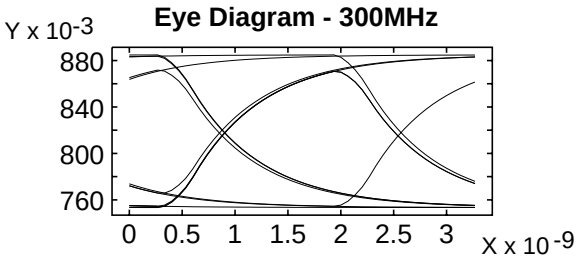

(A) 5μm detectors

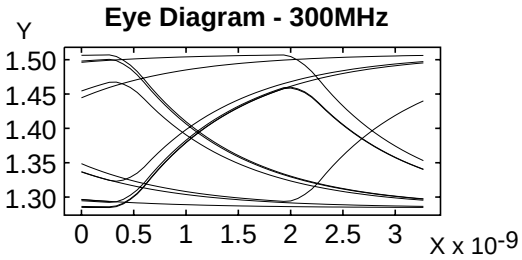

(B) 20μm off-center detectors

Figure 8: Speed vs. Power trade-off

larger ones. For both models, the effective R_f was 6.66KΩ. The choice of which receiver to use, in this case, depends on whether intensity-dependent or intensity-independent noise sources are dominant in these detectors.

4. Summary and Conclusions

We have shown the modeling and simulation of several hybrid opto-electronic free space systems. We used both analytical and empirical models for O/E components and a Gaussian beam propagation model for our optical signals. We performed a static analysis of the system showing the effects of detector size and tolerances on received power. We also showed the effect of mis-alignment and clipping of the light beams. For the dynamics of the system we used a time-domain analysis of the O/E components. The simulations showed how detector size, and alignment can affect the noise margins of the system.

Our system is the only system level simulation tool to date which can model Gaussian optical signal propagation with mechanical tolerancing as well as the dynamics of opto-electronic components. We have not yet modeled the losses and noise sources in the lasers, modulators, and receivers, or cross-talk between signal channels. On the other hand, modulation and coding methods, differential signaling, adaptive thresholding, and other techniques can be used to reduce the bit error rate. It is these kinds of system level concerns and the corresponding trade-offs which can only be modeled with system design tools such as the one presented here. With system level models, designers are able to perform the trade-offs, optimizations, and technology choices necessary to realize high-quality systems without recourse to expensive fabrication testing and iteration using hardware prototypes.

Levitan, Chiarulli, and Kurzweg would like to acknowledge the partial support of NSF Grant MIP-9421777.

5. References

[1] R. A. Athale. *Digital Optical Computing* (Proceedings of SPIE Conference Jan 15-16 1990 Los Angles, CA) Spie Optical Engineering Press, Bellingham, WA, 1990.

[2] J. Buck, S. Ha, E. A. Lee, and D. Messerschmitt, Ptolemy: A Framework for Simulating and Prototyping Heterogeneous Systems**.** *Int. Journal of Computer Simulation,* special issue on "Simulation Software Development", January, 1994.

[3] D. M. Chiarulli, S. P. Levitan, R. G. Melhem, C. Qiao. Locality based control algorithms for reconfigurable optical networks. *Applied Optics,* Vol. 33, No. 8, pp. 1528-1537, 10 March, 1994.

[4] A. S. Daryoush, N. Samant, D. Rhodes, and D. Sturzbecher. Photonic cad for high speed fiber-optic links. *Microwave Journal,* 36(3):58, 61--2, 66--7, 69, March 1993.

[5] J. C. Eble, V. K. De, and J. D. Meindl, A first generation Generic System Simulator (GENESYS) and it's relation to NTRS, in *Tech. Dig. IEEE Eleventh Biennial UGIM Symposium,* Austin, TX., 147-154, May 1995.

[6] J. Fan, B. Catanzaro, F. E. Kiamilev S. C. Esener and S. H. Lee. Architecture of an integrated computer-aided design system for optoelectronics. *Optical Engineering,* vol.33, (no.5):1571-80. 26, May 1994.

[7] C. Fan, B. Mansoorian, D. A. Van Blerkom, M. W. Hansen, V. H. Ozguz, S. C. Esener, and G, C. Marsden. Digital free-space optical interconnections: a comparison of transmitter technologies. *Applied Optics* 34(7) pp. 3103-3115, 10 June 1995.

[8] H. S. Hinton. *An Introduction to Photonic Switching Fabrics.* Plenum Press, New York, 1993.

[9] J. Jewell and G. Olbright. Vertical cavity surface emitting lasers. *IEEE Journal of Quantum Electronics* Vol. 27, 1332-1346 (1991).

[10] S. P. Levitan, P. J. Marchand, M. Rempel, D. M. Chiarulli, F. B. McCormick. Computer-aided design of free-space optoelectronic interconnection (FSOI) systems. In *Second International IEEE Workshop on Massively Parallel Processing Using Optical Interconnections.* 239-245, San Antonio, TX, October 23-24, 1995.

[11] A. Louri, J. Na. Modeling and simulation methodology for digital optical computing systems. *Applied Optics,* vol.33, (no.8):1549-58, 10 March 1994.

[12] A. J. Lowery, P. C. R. Gurney, X-H. Wang, L. V. T. Nguyen, Y-C. Chan, and M. Premaratine. Time-domain simulation of photonic devices, circuits, and systems. Lasers and Integrated Devices Symposium, Photonics West '96, San Jose, CA February 1996.

[13] P. Marchand, A. Krishnamoorthy, G. Yayla, S. Esener, and U. Efron, Optically Augmented 3-D Computer: System Technology and Architecture, *Journal of Parallel and Distributed Computing, Special Issue on Optical Interconnects* (in press).

[14] F. B. McCormick, F. A. Tooley, T. J. Cloonan, J. M. Sasian, and H. S. Hinton. Microbeam optical interconnections using microlens arrays. *Optical Society of America Proceedings on Photonic Switching,* 1991. Vol. 8. H. Scott Hinton and Joseph W. Goodman (eds.).

[15] D. A. B. Miller. Quantum wells for optical information processing. *Optical Engineering* 26 (5), 368-372, May 1987.

[16] M. A. Neifeld and W-C. Chou. Electrical Packaging Impact on Source Components in Optical Interconnects. *IEEE Transactions on Components, Packaging and Manufacturing Technology Part B: Advanced Packaging,* vol.18, (no.3):578-95, Aug. 1995.

[17] B. E. A. Saleh and M.C. Teich, *Fundamentals of Photonics.* Wiley, New York, 1991.

[18] A. T. Yang, D. S. Gao, and S. M. Kang. Computer-aided simulation of optical interconnects for high-speed digital systems. *Proc. 1988 IEEE International Conference on Computer Design.* pp. 87-90, Oct. 1988.

[19] D. Zaleta, S. Patra, V. Ozguz, J. Ma, and S. H. Lee. Tolerancing of board-level-free-space optical interconnects. *Applied Optics.* Vol. 35, No. 8, p. 1317, 10 March 1996.